imaging with incoherent x-rays," *Opt. Rev*, **7**, pp. 566-572, 2000.

5. E. Sato, S. Kimura, S. Kawasaki, H. Isobe, K. Takahashi, Y. Tamakawa and T. Yanagisawa, "Repetitive flash x-ray generator utilizing a simple diode with a new type of energy-selective function," *Rev. Sci. Instrum.*, **61**, pp. 2343-2348, 1990.
6. E. Sato, A. Shikoda, S. Kimura, M. Sagae, T. Oizumi, K. Takahashi, Y. Hayasi, T. Shoji, K. Shishido, Y. Tamakawa and T. Yanagisawa, "Repetitive compact flash x-ray generators for soft radiography," *SPIE*, **1801**, pp. 628-642, 1992.
7. E. Sato, M. Sagae, K. Takahashi, T. Oizumi, H. Ojima, K. Takayama, Y. Tamakawa, T. Yanagisawa, A. Fujiwara and K. Mitoya, "High-speed soft x-ray generators in biomedicine," *SPIE*, **2513**, pp. 649-667, 1994.
8. E. Sato, M. Sagae, K. Takahashi, A. Shikoda, T. Oizumi, H. Ojima, K. Takayama, Y. Tamakawa, T. Yanagisawa, A. Fujiwara and K. Mitoya, "Dual energy flash x-ray generator," *SPIE*, **2513**, pp. 723-735, 1994.
9. A. Shikoda, E. Sato, M. Sagae, T. Oizumi, Y. Tamakawa and T. Yanagisawa, "Repetitive flash x-ray generator having a high-durability diode driven by a two-cable-type line pulser," *Rev. Sci. Instrum.*, **65**, pp. 850-856, 1994.
10. E. Sato, K. Takahashi, M. Sagae, S. Kimura, T. Oizumi, Y. Hayasi, Y. Tamakawa and T. Yanagisawa, "Sub-kilohertz flash x-ray generator utilizing a glass-enclosed cold-cathode triode," *Med. & Biol. Eng. & Comput.*, **32**, pp. 289-294, 1994.
11. K. Takahashi, E. Sato, M. Sagae, T. Oizumi, Y. Tamakawa and T. Yanagisawa, "Fundamental study on a long-duration flash x-ray generator with a surface-discharge triode," *Jpn. J. Appl. Phys.*, **33**, pp. 4146-4151, 1994.
12. E. Sato, M. Sagae, A. Shikoda, K. Takahashi, T. Oizumi, M. Yamamoto, A. Takabe, K. Sakamaki, Y. Hayasi, H. Ojima, K. Takayama and Y. Tamakawa, "High-speed soft x-ray techniques," *SPIE*, **2869**, pp. 937-955, 1996.
13. E. Sato, Y. Suzuki, Y. Hayasi, E. Tanaka, H. Mori, T. Kawai, K. Takayama, H. Ido and Y. Tamakawa, "High-intensity quasi-monochromatic x-ray irradiation from the linear plasma target," *SPIE*, **4505**, pp. 154-164, 2001.
14. E. Sato, Y. Hayasi, E. Tanaka, H. Mori, T. Kawai, T. Usuki, K. Sato, H. Obara, T. Ichimaru, K. Takayama, H. Ido and Y. Tamakawa, "Quasi-monochromatic radiography using a high-intensity quasi-x-ray laser generator," *SPIE*, **4682**, pp. 538-548 2002.
15. E. Sato, Y. Hayasi, E. Tanaka, H. Mori, T. Kawai, K. Takayama and H. Ido, "Irradiation of intense characteristic x-rays from weakly ionized linear plasma," *Proc 3rd Korea-Japan Joint Meeting on Medical Physics, Gyeongju*, pp. 396-399, 2002.
16. A.A. Bzhanmikov, N. Langhoff, J. Schmalz, R. Wedell, V.L. Beloglazov and N.F. Lebedev, "Polycapillary conic collimator for micro-XRF," *SPIE*, **3444**, pp. 430-435, 1998.
17. Q.F. Xiao and S.V. Poturaef, "Polycapillary-based x-ray optics," *Nucl. Instr. Meth. Phys. Res. A*, **347**, pp. 376-383, 1994.
18. E. Sato, Y. Hayasi, E. Tanaka, H. Mori, T. Kawai, H. Obara, T. Ichimaru, K. Takayama, H. Ido, T. Usuki, K. Sato and Y. Tamakawa, "Polycapillary radiography using a quasi-x-ray laser generator," *SPIE*, **4508**, pp. 176-187, 2001.

19. E. Sato, H. Toriyabe, Y. Hayasi, E. Tanaka, H. Mori, T. Kawai, T. Usuki, K. Sato, H. Obara, T. Ichimaru, K. Takayama, H. Ido and Y. Tamakawa,"Fundamental study on parallel beam radiography using a polycapillary plate," *SPIE*, **4682**, pp. 298-310, 2002.
20. E. Sato, Y. Hayasi, T. Usuki, K. Sato, H. Ojima, K. Takayama and H. Ido, "Soft plasma flash x-ray generator utilizing a vacuum discharge capillary," *Proc 3rd Korea-Japan Joint Meeting on Medical Physics, Gyeongju*, pp. 400-403, 2002.

Fundamental study on parallel beam radiography using a polycapillary plate

Eiichi Sato[a], Hiroyuki Toriyabe[a], Yasuomi Hayasi[b], Etsuro Tanaka[c], Hidezo Mori[d], Toshiaki Kawai[e], Tatsumi Usuki[f], Koetsu Sato[f], Haruo Obara[g], Toshio Ichimaru[h], Kazuyoshi Takayama[i], Hideaki Ido[j] and Yoshiharu Tamakawa [k]

[a] Department of Physics, Iwate Medical University, 3-16-1 Honcho-Dori, Morioka 020-0015, Japan
[b] Electrical Engineering, Hachinohe National College of Technology, 16-1 Tamonoki Uwanotai, Hachinohe 039-1104, Japan
[c] Department of Physiology, School of Medicine, Tokai University, Boseidai, Isehara 259-1193, Japan
[d] Department of Cardiac Physiology, National Cardiovascular Center Research Institute, 5-7-1 Fujishiro-dai, Suita, Osaka 565-8565 Japan
[e] Electron Tube Division #2, Hamamatsu Photonics K.K., 314-5 Shimokanzo, Toyooka Village, Iwata-gun 438-0193, Japan
[f] Toreck Inc., Tsunashima Higashi, Kohoku-Ku, Yokohama 223, Japan
[g] Department of Radiological Technology, College of Medical Science, Tohoku University, 1-1 Seiryo-cho, Sendai 980-0872, Japan
[h] Department of Radiological Technology, School of Allied Medical Sciences, Hirosaki University, 66-1 Hon-cho, Hirosaki 036-8564, Japan
[i] Shock Wave Research Center, Institute of Fluid Science, Tohoku University, 1-1 Katahira, Sendai 980-8577, Japan
[j] Department of Applied Physics, Faculty of Engineering, Tohoku Gakuin University, Tagajo 985-0873, Japan
[k] Department of Radiology, Iwate Medical University, 19-1 Uchimaru, Morioka 020-0023, Japan

ABSTRACT

Fundamental study on parallel beam radiography using a polycapillary plate is described. The x-ray generator used in this experiment is NST-1005 made by Sofron Inc. with maximum tube voltage and current of 100 kV (peak value) and 5.0 mA, respectively. In this experiment, the tube voltage was regulated from 20 to 30 kV, and the tube current had a constant value of 4.0 mA. The exposure time is regulated in order to control optimum film density. The polycapillary plate is J5022-21 made by Hamamatsu Photonics, and the outside and effective diameters are 87 and 77 mm, respectively. The thickness and the whole diameter of the polycapillary are 1.0 mm and 25 μm, respectively. The x-rays from the tube are formed to parallel beam by the polycapillary, and the radiogram is taken using an industrial x-ray film of Fuji IX 100 without using a screen. In the measurement of image resolution, we employed three brass spacers of 2, 30, and 60 mm in height. By the test chart, the resolution decreased according to increases in the spacer height without using the polycapillary. In contrast, the resolution seldom varied when the polycapillary was employed. In the polycapillary radiography of four tungsten wires, higher-contrast images of 50 μm wire were observed, and the line width seldom varied according to increases in the spacer height.

1. INTRODUCTION

In conjunction with a single crystal, the synchrotron generates high-dose-rate monochromatic x-rays. These rays have been applied effectively to perform high-contrast angiography, and possible applications[1-3] have been considered in medical radiography for a long time. However, it is difficult to obtain sufficient machine times for various researches.

Medical Imaging 2002: Physics of Medical Imaging, Larry E. Antonuk, Martin J. Yaffe, Editors, Proceedings of SPIE Vol. 4682 (2002) © 2002 SPIE ·1605-7422/02/$15.00

With recent advances in the high-voltage pulse technology, various high-speed x-ray generators[4-19] with x-ray qualities of very soft to hard have been developed corresponding to the radiographic objectives, and generators[4-19] with photon energies of lower than 150 keV have been applied to soft radiographies including biomedical applications. Next, the characteristic x-rays have been amplified by forming the linear plasma x-ray source,[20-22] and we have performed high-speed quasi-monochromatic radiography without using a monochromatic filter. Even when the plasma x-ray generator produces high-intensity quasi-monochromatic x-rays, the optimum x-ray optical system[23,24] is desired in order to increase the image resolution.

In the x-ray optics, although several different x-ray lenses have been developed, a polycapillary plate[21] is useful to realize a low-priced system and to perform parallel beam radiography. In view of this situation, we have been designing the monochromatic parallel radiography system using a polycapillary plate and have already succeeded in creating new monochromatic x-ray tubes. Therefore, we have to measure fundamental radiographic characteristics of the polycapillary plate according to changes in the tube voltage and other conditions using a soft x-ray generator.

In the present work, we have performed fundamental study on parallel beam radiography achieved with a polycapillary plate in order to increase the image resolution of radiography.

2. SETUP

Figure 1 shows a method for performing parallel radiography using a polycapillary plate. The x-ray generator used in this experiment is NST-1005 (Fig. 2) made by Sofron Inc. with maximum tube voltage and current of 100 kV (peak value) and 5.0 mA, respectively. In this experiment, the tube voltage was regulated from 20 to 30 kV, and the tube current had a constant value of 4.0 mA. The exposure time is regulated in order to control the optimum film density. The polycapillary plate is J5022-21 made by Hamamatsu Photonics, and the outer and effective diameters are 87 and 77 mm, respectively. The thickness and the whole diameter of the polycapillary are 1.0 mm and 25 μm, respectively. The x-rays from the tube are formed to parallel beam by the polycapillary, and the radiogram is taken using an industrial x-ray film (Fuji IX 100) without a screen.

The experimental setup is shown in Figs. 3 and 4, and the x-ray tube employs a tungsten target and a beryllium window. The distance between the x-ray focus and film is 0.5 m, and the dimensions of focal spot are about 1×1 mm. The polycapillary plate is placed on the brass spacer, and the radiogram is roughly observed by a setup of screen and mirror.

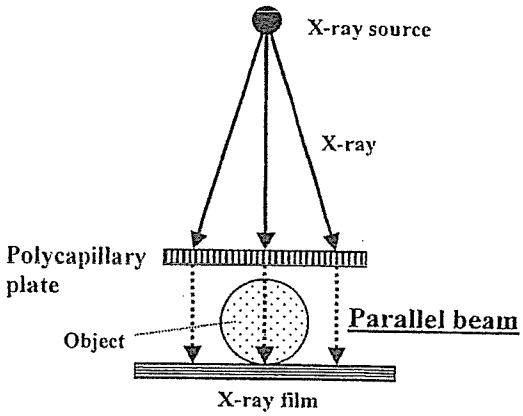

Fig. 1 Parallel beam radiography achieved with a conventional x-ray generator.

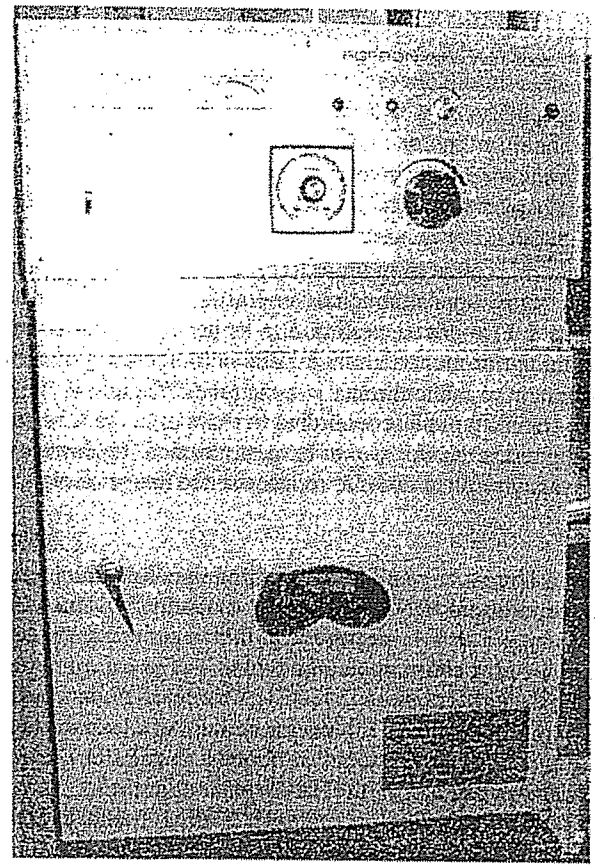

Fig. 2 X-ray generator.

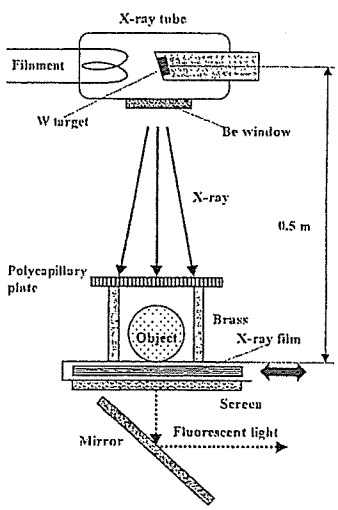

Fig. 3 Experiment setup of the parallel radiography.

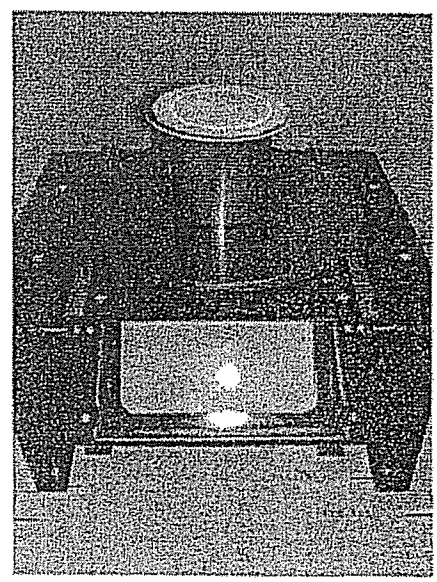

Fig. 4 Inner side of the x-ray generator.

3. RADIOGRAPHY

3.1 Radiography of test chart

The brass spacers, the polymethyl methacrylate (PMMA) spacers, the polycapillary plate, and the test chart for measuring image resolution are shown in Fig. 5. Figure 6 shows radiography for imaging the polycapillary plate, and the radiograms of the polycapillary are shown in Fig. 7. The center of the black spot in the polycapillary is imaged by almost the direct transmission beams through capillary holes. As shown in this figure, both the spot density and the dimension seldom varied according to increases in the brass-spacer height.

In order to image the test chart, we employed the setup shown in Fig. 8. Of course, the image resolution increased according to decreases in the spacer height, and we could observe 100 μm lines clearly with a height of 2 mm (Fig. 9). Figure 10 shows the parallel radiography for imaging the test chart, and the polycapillary was placed on the chart. In this radiography, we observed 100 μm lines clearly even when a higher spacer of 60 mm was employed (Fig. 11). At a constant spacer height (Fig. 12), the image resolution seldom varied with corresponding changes in the tube voltage (Fig. 13).

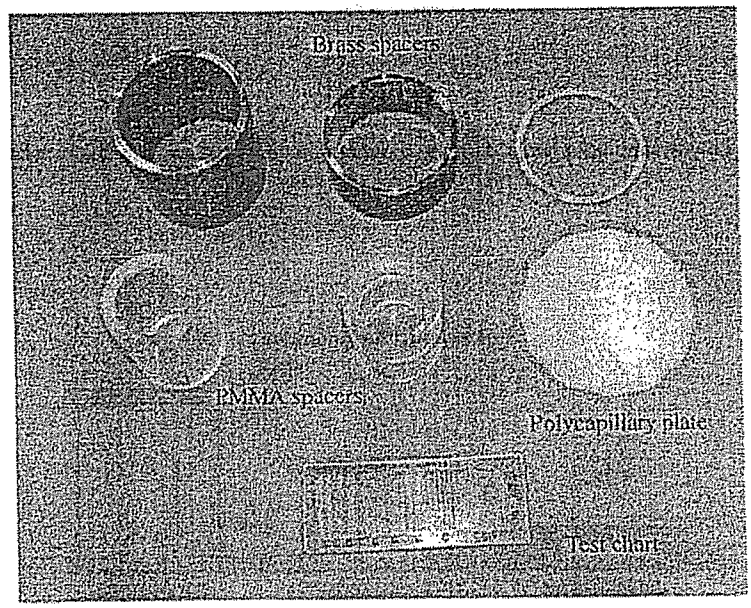

Fig. 5 Experiment instruments.

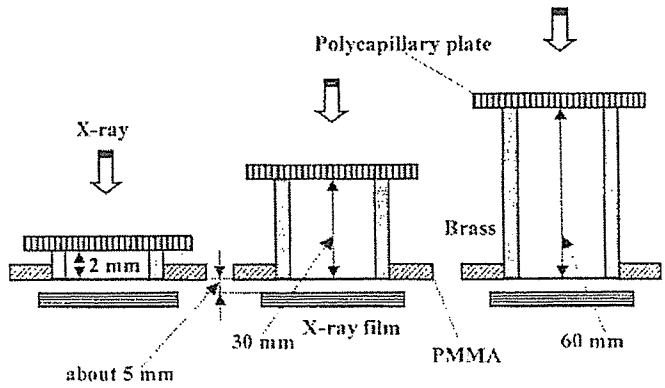

Fig. 6 Radiography of the polycapillary plate.

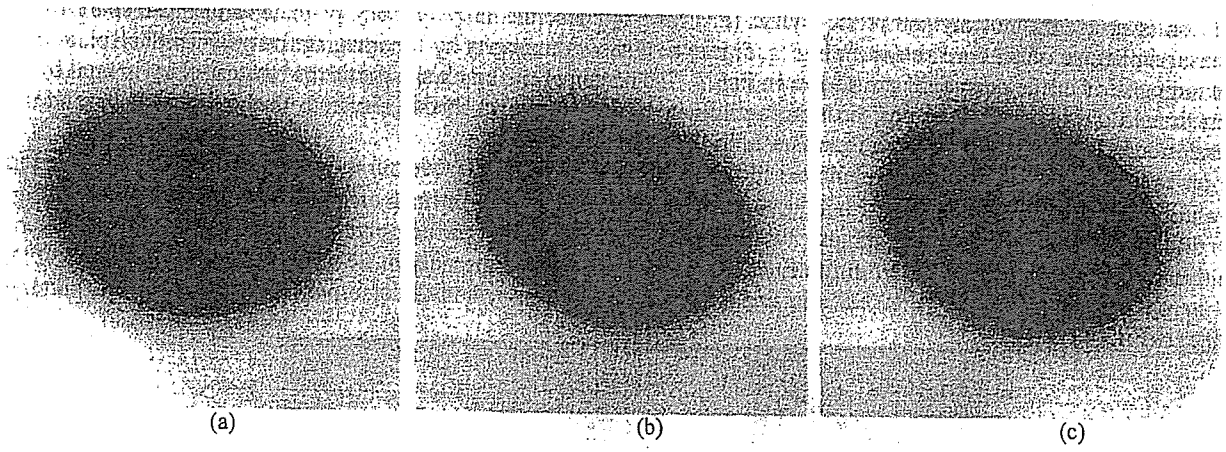

Fig. 7 Radiograms of the polycapillary plate according to changes in the height of brass spacer with a tube voltage of 25 kV: (a) 2 mm, (b) 30 mm, and (c) 60 mm.

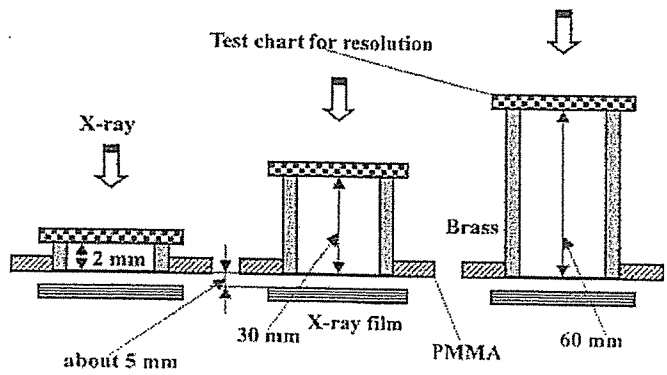

Fig. 8 Radiography of the test chart for measuring image resolution.

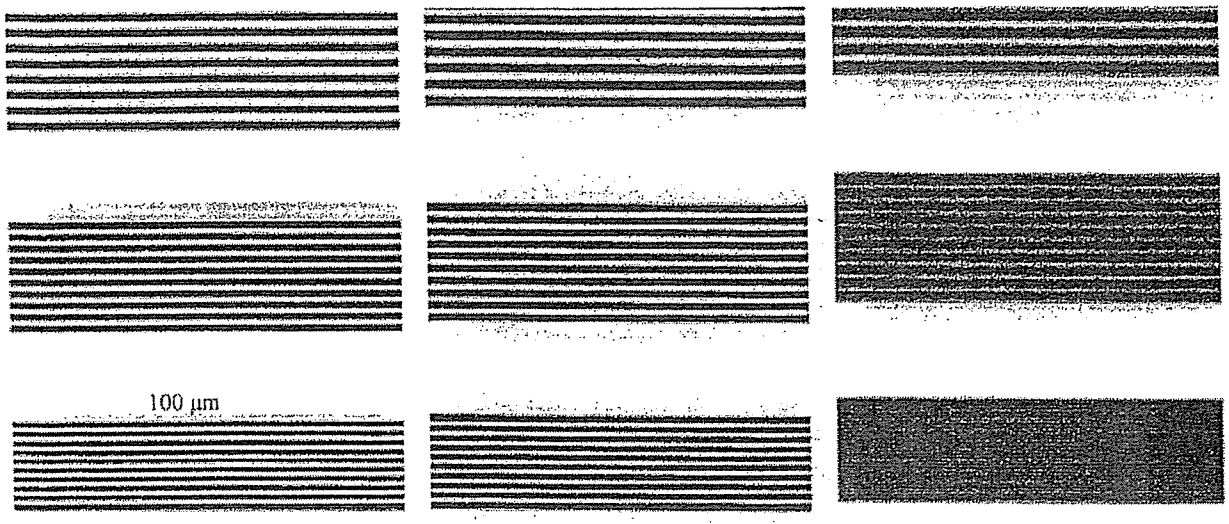

(a) (b) (c)

Fig. 9 Radiograms of the test chart according to changes in the height of the brass spacer at a tube voltage of 25 kV: (a) 2 mm, (b) 30 mm, and (c) 60 mm.

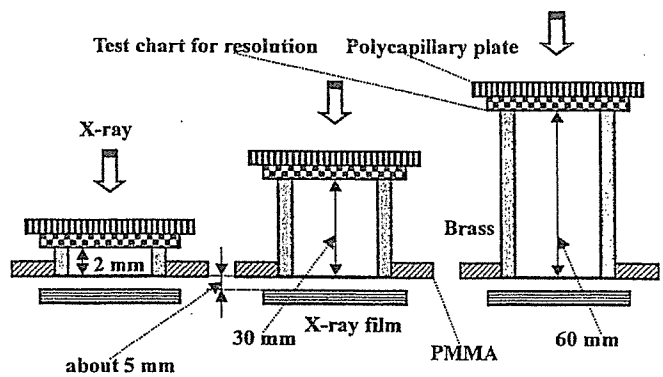

Fig. 10 Radiography of the test chart using the polycapillary plate.

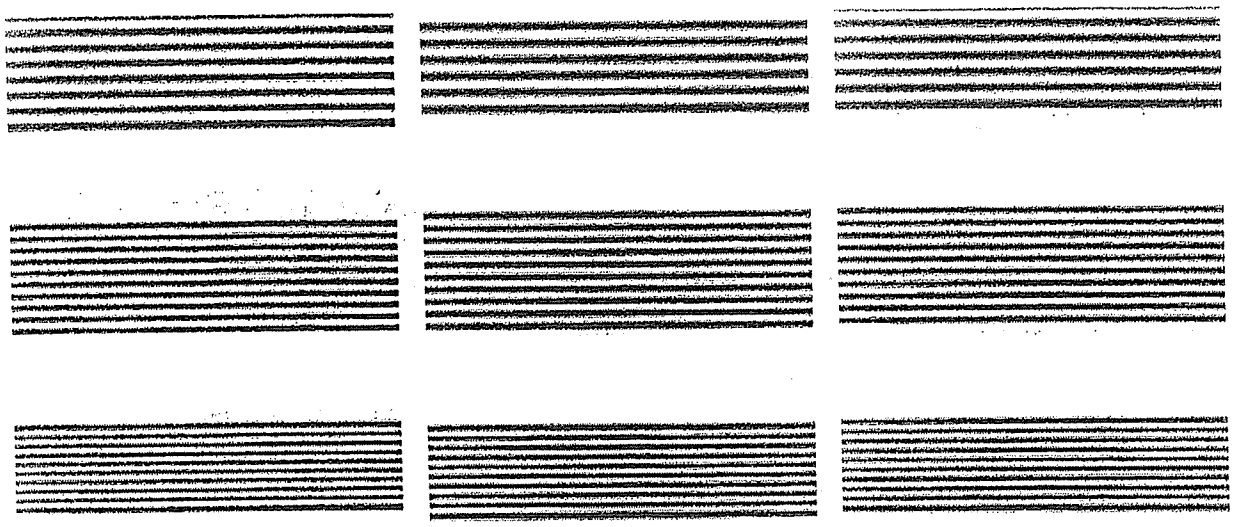

Fig. 11 Radiograms of the test chart according to changes in the height of the brass spacer using the polycapillary plate with a tube voltage of 25 kV: (a) 2 mm, (b) 30 mm, and (c) 60 mm.

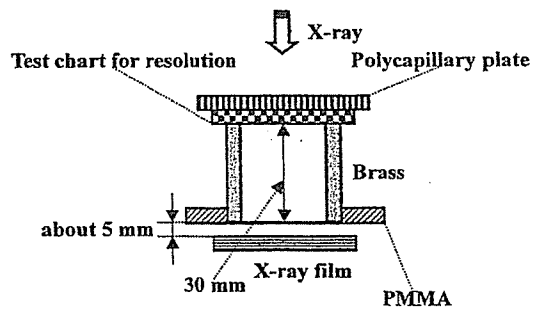

Fig. 12 Experiment instruments for imaging the test chart according to changes in the tube voltage.

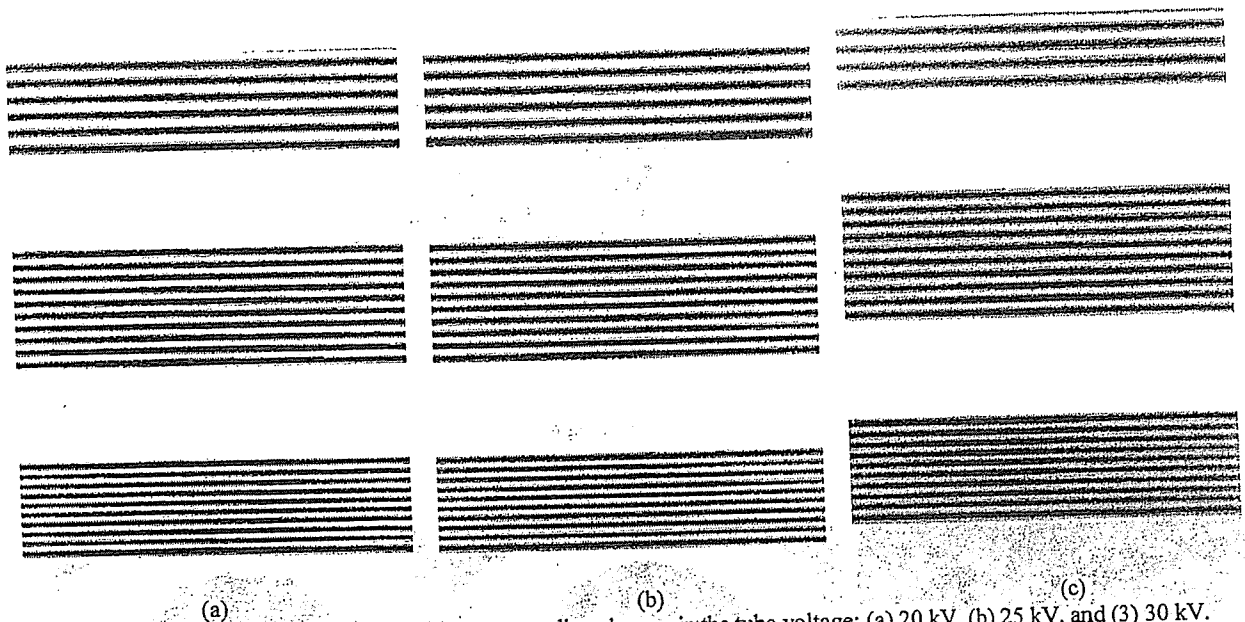

(a) (b) (c)

Fig. 13 Radiograms of the test chart with corresponding changes in the tube voltage: (a) 20 kV, (b) 25 kV, and (3) 30 kV.

3.2 Radiography of tungsten wires

In order to image tungsten wires, we selected four diameters of 300, 200, 100, and 50 μm (Fig. 14). Figure 15 shows the setup for imaging the wires, and two kinds of PMMA spacers were employed. In this radiography, tungsten wires were placed on the polyethylene terephthalate (Mylar) film of 100 μm. When the spacer height was increased, the image contrast decreased, and the image of 50 μm line disappeared (Fig. 16). Using the polycapillary, the four lines were visible even when the spacer height increased (Figs. 17 and 18).

The variation of resolution with the PMMA thickness is important, and two PMMA spacers were employed to perform radiography (Fig. 19). As shown in Fig. 20, we observed lower-contrast four lines. Next, of course, four lines were observed by the polycapillary plate (Figs. 21 and 22), and widths had smaller values compared with those obtained without using the polycapillary.

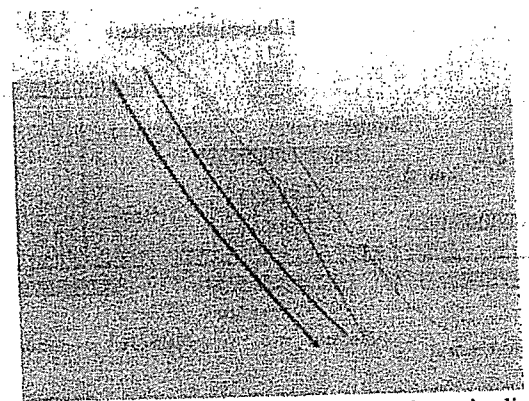

Fig. 14 Tungsten wires of 300, 200, 100, and 50 μm in diameter.

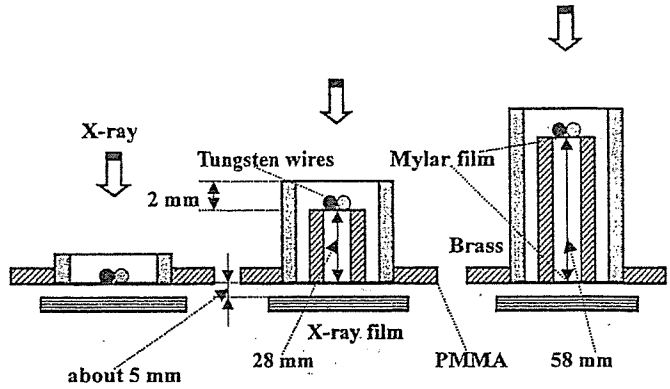

Fig. 15 Radiography for imaging tungsten wires.

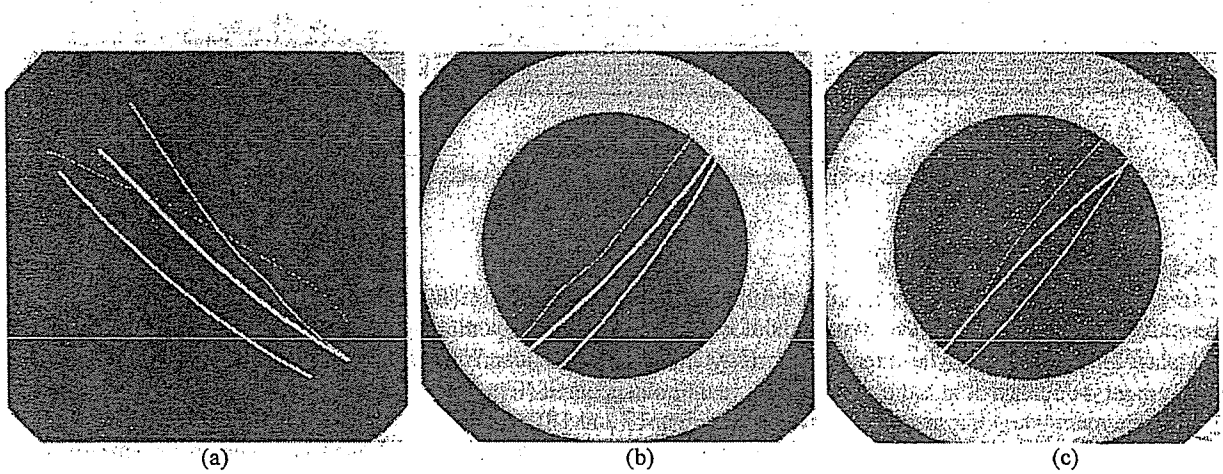

Fig. 16 Radiograms of the wires according to changes in the height of brass spacer at a tube voltage of 25 kV: (a) 2 mm, (b) 30 mm, and (c) 60 mm.

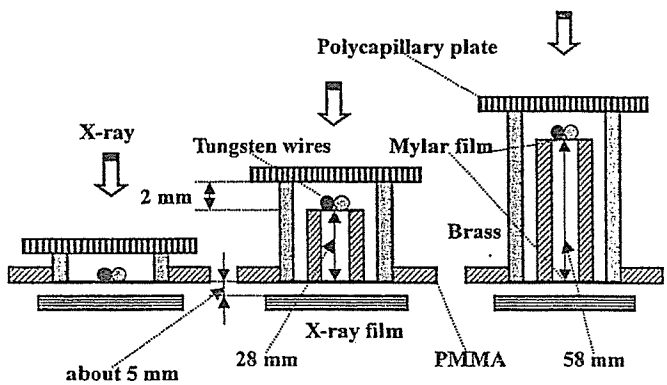

Fig. 17 Radiography of tungsten wires using the polycapillary plate.

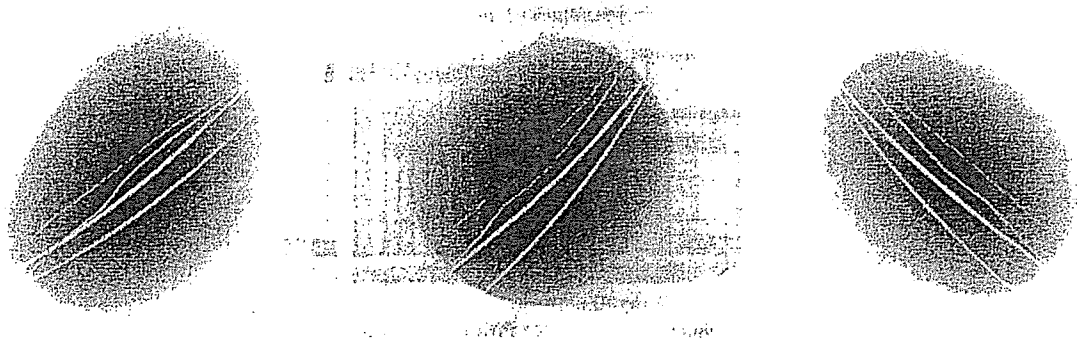

(a) (b) (c)

Fig. 18 Radiograms of wires according to changes in the height of brass spacer using the polycapillary plate with a tube voltage of 25 kV: (a) 2 mm, (b) 30 mm, and (c) 60 mm.

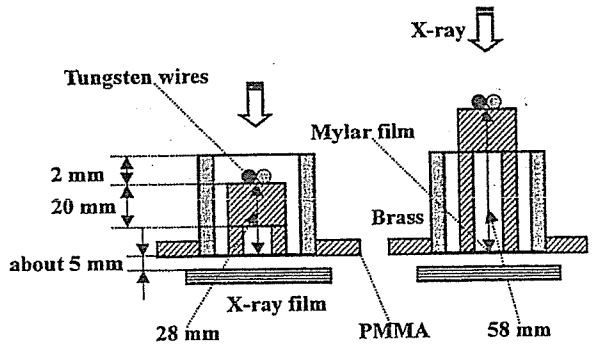

Fig. 19 Radiography of tungsten wires using a 20 mm PMMA spacer.

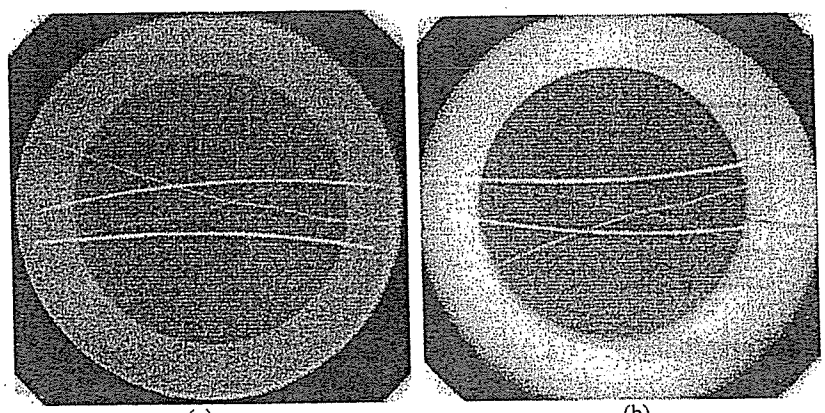

(a) (b)

Fig. 20 Radiograms of the wires according to changes in the height of PMMA spacer with a tube voltage of 30 kV: (a) 30 mm and (b) 60 mm.

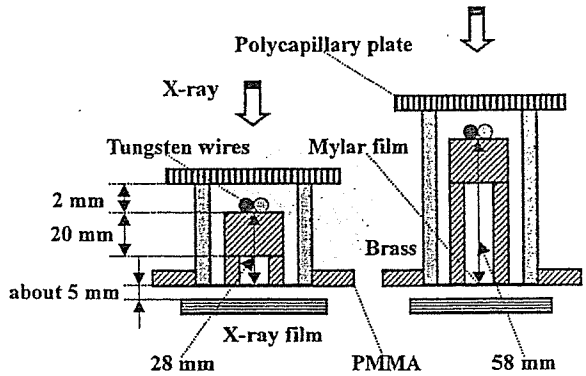

Fig. 21 Radiography of the tungsten wires achieved with the polycapillary plate and a 20 mm PMMA spacer.

Fig. 22 Radiograms of the wires according to changes in the height of PMMA spacer using the polycapillary plate at a tube voltage of 30 kV: (a) 30 mm and (b) 60 mm.

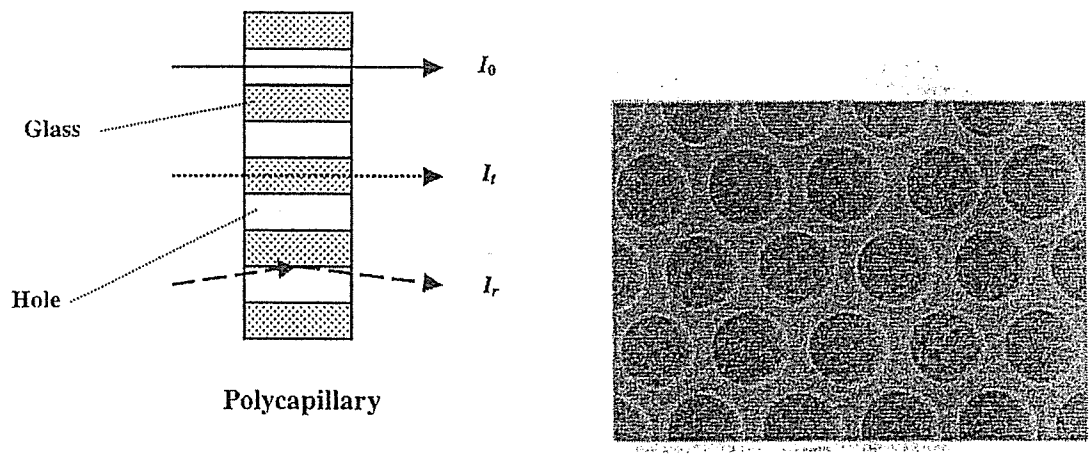

Fig. 23 X-ray penetration of polycapillary plate.

4. DISCUSSION

Using this polycapillary, we have obtained higher image resolutions and contrasts, and the resolution increases with corresponding decreases in the hole diameter of the polycapillary. When a polycapillary plate is employed, the x-ray intensity without absorbing I_0, transmission intensity I_t, and the reflecting intensity I_r may be given by (Fig. 20):

$$I_0 = K_1 \int_0^{\infty} I(E)\,dE, \tag{1}$$

$$I_t \cong K_2 \int_0^{\infty} I(E) \cdot \exp\{-\mu(E) \cdot a\}\ dE, \tag{2}$$

$$I_r = K_3 \int_0^{\phi} \int_0^{\infty} I(E) \cdot R(E,\theta)^n\ dE\ d\theta, \tag{3}$$

where $I(E)$ is the spectrum distribution from the x-ray tube including tungsten L-series characteristic x-rays, ϕ is the critical angle of total reflection, $R(E, \theta)$ is the reflecting power ($1 \geq R(E, \theta) \geq 0$) as functions of photon energy E and incident angle θ, n is the reflecting number, $\mu(E)$ is the linear absorption coefficient of polycapillary glass, a is the polycapillary thickness, and $K_1 \sim K_3$ are constants. Thus the x-ray spectrum distribution varies according to changes in the reflection number and the glass thickness. Next, the critical angle is given by:

$$\phi = \sin^{-1}\{\lambda (e^2 N / \pi m c^2)^{0.5}\}, \tag{4}$$

where λ is the wave length, e is the electron charge, N is the electron number per unit volume, m is the electron mass, and c is the light velocity. Thus the angle increases according to increases in the wave length. In the parallel radiography, because the transmission intensity is not required, the total intensity for parallel radiography I is represented by:

$$I = I_0 + I_r >> I_t. \tag{5}$$

At a constant incident angle, because the reflecting intensity is approximated, and the spectrum distribution $I_p(E)$ for parallel radiography is roughly written by:

$$I_r \cong K_3 \int_0^{\infty} I(E) \cdot R(E)^n\ dE, \tag{6}$$

$$I_p(E) \cong I(E)\{K_1 + K_3 R(E)^n\}. \tag{7}$$

For this research, we have performed parallel beam radiography achieved with a polycapillary plate in conjunction with a conventional x-ray generator. However, the irradiation field is very narrow compared with those obtained by the conventional x-ray generator that produces cone beams. Therefore, a monochromatic plane-focus x-ray tube is needed in order to increase the irradiation field and to perform higher contrast angiography.

ACKOWLEDGEMENTS

This work was supported by Grants-in-Aid for Scientific Research (12670902, 13470154 and 13877114) from MECSST, Japan Science and Technology Corporation, Scientific Research from New Energy and Industrial Technology Development Organization, and Cardiovascular Disease (H13C-1) from MHLW.

REFERENCES

1. H. Mori, K. Hyodo, E. Tanaka, et al., "Small-vessel radiography in situ with monochromatic synchrotoron radiation," *Radiology*, **201**, pp. 173-177, 1996.
2. Y. Nakajima, E. Sato, K. Tanioka, T. Kawai, E. Tanaka, W. Kobayashi, Y. Yamamoto, M. Fujii, Y. Shonozaki, Y. Kan, K. Hyodo, M. Ando and H. Mori, "Possible application of plasma x-ray source to clinical radiography," *SPIE*, **4183**, pp. 365-372, 2000.

3. M. Ando and H. Sugiyama, "X-ray trichromator "Trinity" and x-ray dark field camera "Owl"," *Rigaku-Denki J.*, 32(2), pp. 16-27, 2001.
4. R. Germer, "X-ray flash techniques," *J. Phys. E: Sci. Instrum.*, **12**, pp. 336-350, 1979.
5. E. Sato, S. Kimura, S. Kawasaki, H. Isobe, K. Takahashi, Y. Tamakawa and T. Yanagisawa, "Repetitive flash x-ray generator utilizing a simple diode with a new type of energy-selective function," *Rev. Sci. Instrum.*, **61**, pp. 2343-2348, 1990.
6. E. Sato, A. Shikoda, S. Kimura, M. Sagae, H. Isobe, Y. Tamakawa and T. Yanagisawa, "Kilohertz-range flash x-ray generator utilizing a triode in conjunction with an extremely hot cathode," *Rev. Sci. Instrum.*, **62**, pp. 2115-2120, 1991.
7. E. Sato, M. Sagae, K. Takahashi, A. Shikoda, T. Oizumi, Y. Hayasi, Y. Tamakawa and T. Yanagisawa, "10 kHz microsecond pulsed x-ray generator utilizing a hot-cathode triode with variable durations for biomedical radiography," *Med. & Biol. Eng. & Comput.*, **32**, pp. 295-301, 1994.
8. E. Sato, M. Sagae, K. Takahashi, T. Oizumi, H. Ojima, K. Takayama, Y. Tamakawa, T. Yanagisawa, A. Fujiwara and K. Mitoya, "High-speed soft x-ray generators in biomedicine," *SPIE*, **2513**, pp. 649-667, 1994.
9. E. Sato, K. Takahashi, M. Sagae, S. Kimura, T. Oizumi, Y. Hayasi, Y. Tamakawa and T. Yanagisawa, "Sub-kilohertz flash x-ray generator utilizing a glass-enclosed cold-cathode triode," *Med. & Biol. Eng. & Comput.*, **32**, pp. 289-294, 1994.
10. K. Takahashi, E. Sato, M. Sagae, T. Oizumi, Y. Tamakawa and T. Yanagisawa, "Fundamental study on a long-duration flash x-ray generator with a surface-discharge triode," *Jpn. J. Appl. Phys.*, **33**, pp. 4146-4151, 1994.
11. E. Sato, M. Sagae, K. Takahashi, T. Ichimaru, A. Wataru, S. Kumagai, H. Ido, K. Sakamaki, K. Takayama and Y. Tamakawa, "Monochromatic plasma x-ray generator and its applications," *SPIE*, **3336**, pp. 75-86, 1998.
12. K. Takahashi, E. Sato, M. Sagae and Y. Tsukahara, "Semi-monochromatic plasma flash radiography and its application to biomedical image simulation," *Jpn. J. Appl. Phys.*, **37**, pp. 4222-4227, 1998.
13. E. Sato. T. Ichimaru, H. Ojima, K. Takayama, H. Ido and Y. Tamakawa, "Characteristics of the kilohertz-range harder stroboscopic x-ray generator and applications," *SPIE*, **3771**, pp. 12-21, 1999.
14. E. Sato, M. Sagae, T. Ichimaru, Y. Hayasi, H. Ojima, K. Takayama, H. Ido, K. Sakamaki and Y. Tamakawa, "Tentative study on x-ray enhancement by fluorescent emission of radiation by plasma x-ray source," *SPIE*, **3771**, pp. 51-60, 1999.
15. E. Sato, Y. Hayasi, H. Mori, E. Tanaka, K. Takayama, H. Ido, K. Sakamaki and Y. Tamakawa, "Quasi-monochromatic x-ray production from the cerium target," *SPIE*, **4142**, pp. 17-28, 2000.
16. E. Sato, T. Ichimaru, H. Obara, M. Zuguchi, H. Mori, E. Tanaka, T. Usuki, K. Sato, H. Ojima, K. Takayama, K. Sakamaki and Y. Tamakawa, "Condenser-discharge stroboscopic x-ray generator for medical radiography," *SPIE*, **4183**, pp. 383-393, 2000.
17. E. Sato, H. Ojima, K. Takayama, M. Matsumasa, H. Obara, M. Zuguchi, T. Usuki, K. Sato, K. Sakamaki and Y. Tamakawa, "Observation of cavitation bubble cloud using a stroboscopic x-ray generator," *SPIE*, **4183**, pp. 394-404, 2000.
18. E. Sato, Y. Hayasi and Y. Tamakawa, "Recent stroboscopic x-ray generators and their applications to high-speed radiography," *Ann. Rep. Iwate Med. Univ. Lib. Arts and Sci.*, **35**, pp. 1-11, 2000.
19. E. Sato, Y. Hayasi, T. Ichimaru, H. Mori, E. Tanaka, H. Ojima, K. Takayama, T. Usuki, K. Sato, K. Sakamaki and Y. Tamakawa, "Tentative study on high-photon-energy quasi-x-ray laser generator by forming plasma x-ray source," *SPIE*, **4183**, pp. 326-338, 2000.
20. E. Sato, Y. Suzuki, Y. Hayashi, E. Tanaka, H. Mori, T. Kawai, K. Takayama, H. Ido and Y. Tamakawa, "High-intensity quasi-monochromatic x-ray irradiation from the linear plasma target," *SPIE*, **4505**, pp. 154-164, 2001.
21. E. Sato, Y. Hayasi, E. Tanaka, H. Mori, T. Kawai, H. Obara, T. Ichimaru, K. Takayama, H. Ido, T. Usuki, K. Sato and Y. Tamakawa, "Polycapillary radiography using a quasi-x-ray laser generator," *SPIE*, **4508**, pp. 176-187. 2001.
22. E. Sato, Y. Hayasi, H. Ojima, K. Takayama and Y. Tamakawa, "High photon energy quasi-x-ray laser generator for shock wave research," *Proc. 23rd Symp. on Shock Waves, Fort Worth*, 2001, to be published.
23. Q.F. Xiao and S.V. Poturaef, "Polycapillary-based x-ray optics," *Nucl. Instr. Meth. Phys. Res. A*, **347**, pp. 376-383, 1994.
24. A.A. Bzhanmikov, N. Langhoff, J. Schmalz, R. Wedell, V.L. Beloglazov and N.F. Lebedev, "Polycapillary conic collimator for micro-XRF," *SPIE*, **3444**, pp. 430-435, 1998.

SWAP-70 is a guanine-nucleotide-exchange factor that mediates signalling of membrane ruffling

Masahiro Shinohara*, Yoh Terada*¶, Akihiro Iwamatsu†, Azusa Shinohara†, Naoki Mochizuki‡¶, Maiko Higuchi§, Yukiko Gotoh§, Sayoko Ihara*, Satoshi Nagata*¶, Hiroshi Itoh*, Yasuhisa Fukui* & Rolf Jessberger||

** Department of Applied Biological Chemistry, Faculty of Agricultural and Life Science, University of Tokyo, Yayoi 1-1-1, Bunkyo-ku, Tokyo 113-8657, Japan*
† Central Laboratories for Key Technology, Kirin Brewery, 1-13-5 Fukuura, Kanazawa-ku, Yokohama City, Kanagawa 236-0004, Japan
‡ Department of Pathology, International Medical Center of Japan, 1-21-1 Toyama, Shinjuku-ku, Tokyo 162-8640, Japan
§ Institute of Molecular and Cellular Biosciences, University of Tokyo, 1-1-1 Yayoi, Bunkyo-ku, Tokyo 113-0032, Japan
|| Mount Sinai School of Medicine, The Carl C. Icahn Institute for Gene Therapy and Molecular Medicine, 1425 Madison Avenue, Box 1496, New York, New York 10029-6574, USA

Phosphoinositide-3-OH kinase (PI(3)K), activated through growth factor stimulation, generates a lipid second messenger, phosphatidylinositol-3,4,5-trisphosphate (PtdIns(3,4,5)P_3)[1–5]. PtdIns(3,4,5)P_3 is instrumantal in signalling pathways that trigger cell activation, cytoskeletal rearrangement, survival and other reactions. However, some targets of PtdIns(3,4,5)P_3 are yet to be discovered[1–7]. We demonstrate that SWAP-70, a unique signalling protein[8–10], specifically binds PtdIns(3,4,5)P_3. On stimulation by growth factors, cytoplasmic SWAP-70, which is dependent on PI(3)K but independent of Ras, moved to cell membrane rearrangements known as ruffles. However, mutant SWAP-70 lacking the ability to bind PtdIns(3,4,5)P_3 blocked membrane ruffling induced by epidermal growth factor or platelet-derived growth factor. SWAP-70 shows low homology with Rac-guanine nucleotide exchange factors (GEFs), and catalyses PtdIns(3,4,5)P_3-dependent guanine nucleotide exchange to Rac. SWAP-70-deficient fibroblasts showed impaired membrane ruffling after stimulation with epidermal growth factor, and failed to activate Rac fully. We conclude that SWAP-70 is a new type of Rac-GEF which, independently of Ras, transduces signals from tyrosine kinase receptors to Rac.

SWAP-70 was originally identified as a protein involved in B-cell activation and heavy-chain immunoglobulin class switching[8,9]. It is abundantly expressed in activated B lymphocytes and in immature mast cells. SWAP-70 localizes to the cytoplasm in these cells, but in B cells it also translocates to the nucleus after appropriate stimulation, which is consistent with a role in immunoglobulin class switching. This translocation, the association of SWAP-70 with the B-cell antigen receptor complex and motifs such as its pleckstrin homology (PH) domain, indicated that SWAP-70 might be involved in signal transduction. The protein has not been detected in the nucleus of a large variety of other cell types or tissues, but the presence of low amounts of SWAP-70 in the cytoplasm of other cell types has not been excluded[8–10]. Mice that are deficient in SWAP-70 are phenotypically healthy but their B cells are hypersensitive to γ-irradiation, show compromised CD40 signalling, and show impaired switching to the immunoglobulin-ε (IgE) class[11]. The signalling pathways within which SWAP-70 acts and its mechanism of action are poorly understood.

PI(3)K is activated immediately upon stimulation of a variety of cells with growth or differentiation factors. Its major product, PtdIns(3,4,5)P_3, is a lipid second messenger that is important in various signalling pathways, including triggering of vesicle transport, cytoskeletal rearrangement and cell survival[1–5]. PI(3)K can be activated by binding to various proteins such as tyrosine-phosphorylated growth-factor receptors, tyrosine-phosphorylated non-receptor cytoplasmic proteins, βγ subunits of trimeric G proteins, or activated Ras[6]. Several laboratories have explored the targets of PI(3)K and have identified some PtdIns(3,4,5)P_3-binding proteins that might be substrates for PtdIns(3,4,5)P_3 modification[6,7]. Considering the functional multiplicity of PI(3)K, a significant number of unknown PtdIns(3,4,5)P_3 targets probably remain to be discovered[7]. We therefore searched for PtdIns(3,4,5)P_3-binding proteins by affinity chromatography on PtdIns(3,4,5)P_3 analogue beads[12].

Total cell lysate from bovine brain was mixed with the beads, and the bound proteins were analysed. Free PtdIns(3,4,5)P_3 enhanced the specificity of binding, which can be competed for by further increased PtdIns(3,4,5)P_3. This approach allowed us to identify several known PtdIns(3,4,5)P_3-binding proteins such as Akt/protein kinase B, PtdIns(3,4,5)P_3-binding protein and Gap1^m (refs 12,13,14,15). However, a protein with a relative molecular mass of 70,000 (M_r70K) seemed to be unknown (Fig. 1a). PtdIns(3,4)P_2 and PtdIns(4,5)P_2 did not block binding of the M_r 70K protein to the PtdIns(3,4,5)P_3 beads, indicating that binding is specific for PtdIns(3,4,5)P_3. Peptide sequences of the purified protein showed

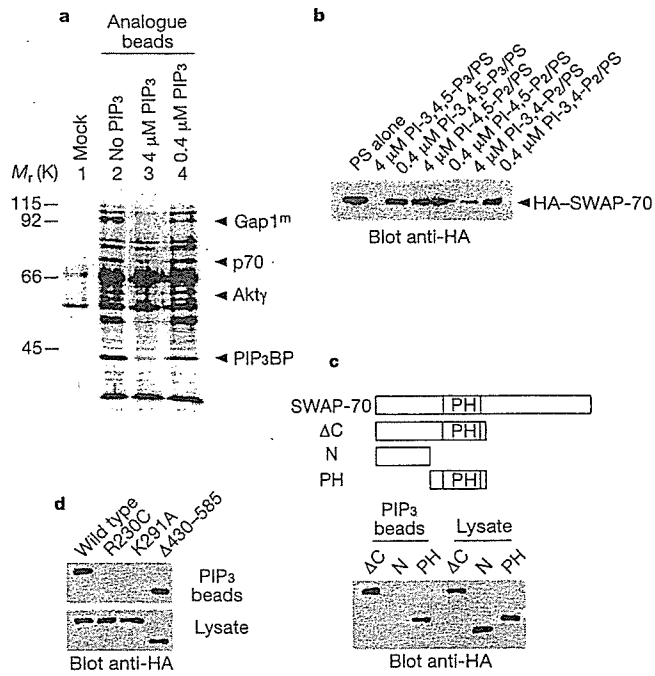

Figure 1 SWAP-70 binds PtdIns(3,4,5)P_3. **a**, Bovine brain lysate was incubated with (0.4 or 4 μM) or without PtdIns(3,4,5)P_3 (PIP$_3$), and mixed with PtdIns(3,4,5)P_3 analogue beads[12]. Bead-bound proteins were analysed by SDS–polyacrylamide gel electrophoresis and silver staining. Mock, beads without PtdIns(3,4,5)P_3; PIP3BP, PtdIns(3,4,5)P_3-binding protein. **b**, Specificity of binding. Lysates prepared from 293T cells expressing HA–SWAP-70 were incubated with phosphoinositides as indicated (PS, phosphatidylserine) and then with PtdIns(3,4,5)P_3-beads. Anti-HA antibody detected bead-bound SWAP-70. **c**, PH domain is required. HA–SWAP-70 deletion mutants were expressed in 293T cells and tested for binding to PtdIns(3,4,5)P_3. ΔC, mutant with deleted C-terminal region; N, N-terminal region of SWAP-70. **d**, As in **c** but with HA–SWAP-70 bearing different point mutations in the PH domain. Δ430–585, amino acids 430–585 deleted.

¶ Present addresses: Molecular Medicine Laboratories, Institute for Drug Discovery Research, Yamanouchi Pharmaceutical Co. Ltd, Tsukuba, Ibaraki 305-8585, Japan (Y.T.); Department of Structure Analysis, National Cardiovascular Center Research Institute, 5-7-4 Fujishirodai, Suita, Osaka 565-8565, Japan (N.M.); Laboratory of Molecular Biology, National Cancer Institute, National Institute of Health, Bethesda, Maryland 20892-4255, USA (S.N.).

almost perfect identity to mouse and human SWAP-70, suggesting that p70 is its bovine homologue (Supplementary Information Fig. S1). Although SWAP-70 expression in brain has not been reported, this tissue also contains a large number of mast cells[16] that might have facilitated the detection of SWAP-70 in the total brain lysate.

SWAP-70 was expressed in 293T cells and subjected to the PtdIns(3,4,5)P_3-binding assay. SWAP-70, tagged with the influenza virus haemagglutinin (HA) epitope, bound efficiently to the PtdIns(3,4,5)P_3 beads (Fig. 1b). Preincubation with other polyphosphoinositides such as PtdIns(3,4)P_2 and PtdIns(4,5)P_2 did not effectively block the binding. Mutational analysis determined that SWAP-70 binds to PtdIns(3,4,5)P_3 as long as it contains the PH domain. Two point mutations in the PH domain, the R230C mutant analogous to that found in Btk of mice with X-linked immunodeficiency[17], and K291A, both abolished the binding of PtdIns(3,4,5)P_3 (Fig. 1c, d). Thus, the PH domain of SWAP-70 is essential for PtdIns(3,4,5)P_3 binding.

To determine the subcellular localization of SWAP-70, the protein was fused to green fluorescent protein (GFP) and was expressed in NIH 3T3 cells. GFP–SWAP-70 was localized mainly in the cytosol (Fig. 2a; Supplementary Information Fig. S2). We examined the behaviour of SWAP-70 upon stimulation with growth factor, which also activates PI(3)K (ref. 5). GFP–SWAP-70 was localized together with actin filaments at membrane ruffles 3 min after stimulation with platelet-derived growth factor (PDGF); 30 min after stimulation, membrane ruffling declined and SWAP-70 returned to the cytosol, suggesting that the translocation of SWAP-70 is reversible (Supplementary Information Fig. S3). The PI(3)K inhibitor wortmannin completely inhibited this reaction. Mutant SWAP-70 protein lacking the ability to bind PtdIns(3,4,5)P_3 not only failed to localize with actin filaments but also blocked membrane ruffling, as did a mutant lacking the carboxy-terminal region. Similar effects were observed in COS7, Chinese hamster ovary and Madin–Darby canine kidney cells stimulated with epidermal growth factor (EGF), insulin and hepatocyte growth factor, respectively (Fig. 2b; Supplementary Information Fig. S2b; and data not shown). These results indicate that SWAP-70 might be required for the formation of membrane ruffles.

Ras-activated PI(3)K is known to induce membrane ruffling through Vav, Sos and Tiam1, that is, PtdIns(3,4,5)P_3-dependent Rac-GEFs[18–20]. However, PI(3)K can also be activated to induce membrane ruffling independently of Ras by binding to tyrosine-phosphorylated growth-factor receptors or to proteins that have been tyrosine-phosphorylated by growth-factor receptors[21–23]. To test whether SWAP-70 signalling is dependent on Ras, dominant-negative Ras was expressed together with SWAP-70 and membrane ruffling was tested. Expression of Ras was readily detectable (data not shown). However, the dominant-negative Ras did not affect membrane ruffling (Fig. 2c; Supplementary Information Fig. S2c).

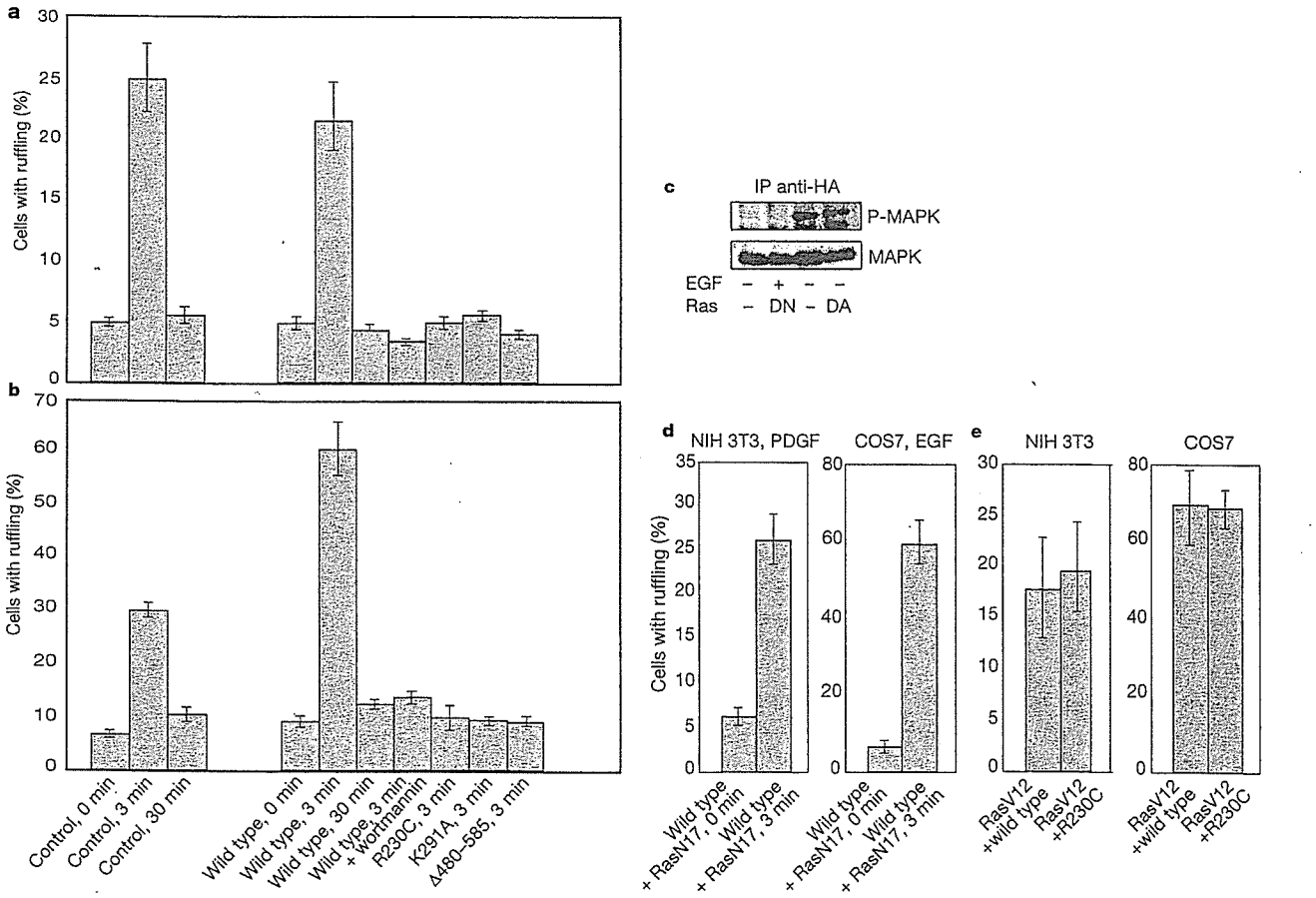

Figure 2 SWAP-70 translocates to membrane ruffles. **a**, **b**, SWAP-70 translocates to membrane ruffles after growth-factor treatment. NIH 3T3 (**a**) or COS7 (**b**) cells, expressing wild-type or mutant GFP–SWAP-70, were stimulated with PDGF (10 ng ml^{-1}) (**a**) or EGF (100 ng ml^{-1}) (**b**) and stained for F-actin: In one experiment, cells were pretreated for 30 min with 100 nM wortmannin. **c**, Dominant-negative Ras blocks the Ras pathway completely. COS7 cells were transfected with or without expression vectors for RasV12 and RasN17. Cells were treated with EGF (100 ng ml^{-1}) for 3 min and the phosphorylation of MAP kinase was analysed by western blotting with anti-phospho-MAP kinase antibody. The lower panel shows expression of MAP kinase detected by western blotting with anti-MAP kinase antibody. **d**, RasN17 does not block membrane ruffling in NIH 3T3 or COS7 cells. IP, immunoprecipitation. **e**, Dominant-negative SWAP-70 does not inhibit membrane ruffling induced by RasV12. Cells with membrane ruffles were scored and normalized to all fluorescent cells. Means for three independent experiments are shown; bars indicate s.d.

Under identical conditions, dominant-negative Ras completely inhibited the activation of MAPK after treatment with EGF in COS7 cells, indicating that the activity of endogenous Ras was completely blocked (Fig. 2d). These results confirm that a growth-factor signalling pathway triggering actin rearrangement independently of the activation of Ras is present in NIH 3T3 or COS7 cells. Expression of constitutively activated Ras resulted in an induction of membrane ruffling. However, flattening of the cells was observed and membrane ruffling was seen on the edge of the cells, which was somewhat different from ruffling seen after stimulation with growth factors, suggesting that constitutively activated Ras does not completely mimic the effect of stimulation with growth factor. Mutant SWAP-70 that lacks PtdIns(3,4,5)P_3-binding activity did not inhibit Ras-induced membrane ruffling (Fig. 2e; Supplementary Information Fig. S2d). This contrasts with membrane ruffling generated by stimulation with PDGF or EGF (Fig. 2a, b), and also shows that SWAP-70 transduces signals from growth-factor receptors independently of Ras.

Examination of the SWAP-70 amino-acid sequence revealed that the C-terminal portion of SWAP-70 has limited similarity to Dbl homology (DH) domains. The putative DH domain of SWAP-70 is 18.1%, 18.7% and 23.2% identical to that of Vav1, Sos1 and Tiam1, respectively[18–20]. By comparison, the DH domain of Vav1 is 27.2% and 24.6% similar to that of Tiam1 and Sos1, respectively (Supplementary Information Fig. S4). However, the DH domain of SWAP-70 is flanked at its amino terminus by the PH domain. This differs from other Rac-GEFs, which have C-terminal PH domains, and underscores the uniqueness of SWAP-70. The GEF activity of SWAP-70 was analysed *in vitro* by monitoring the release of [^{3}H]GDP from purified glutathione *S*-transferase (GST)–Rac1. The rate of [^{3}H]GDP release was slightly enhanced by the presence of SWAP-70 (Fig. 3a). Although it has been reported that PtdIns(3,4,5)P_3 alone stimulates the dissociation of GDP from Rac[24], PtdIns(3,4,5)P_3 was not effective in releasing GDP. However, the addition of both SWAP-70 and PtdIns(3,4,5)P_3 greatly enhanced GEF activity (Fig. 3a). In contrast, SWAP-70 did not show GEF activity on RhoA (Fig. 3b) or Cdc42 (Fig. 3c). An interaction between SWAP-70 and Rac1 was further illustrated by the specific binding of SWAP-70 to Rac1 in absence of Mg^{2+}, but not to RhoA or Cdc42. SWAP-70 bound weakly to GDP-loaded Rac1 but not to GTP-γS-loaded Rac1 (Fig. 3d). This supports the idea that SWAP-70 is a Rac-specific GEF. The R230C mutant lacking PtdIns(3,4,5)P_3-binding activity exhibited wild-type-like GEF activity, but it was not enhanced by the addition of PtdIns(3,4,5)P_3 (Supplementary Information Fig. S5a). Phosphatidylserine, PtdIns, PtdIns(3)P, PtdIns(4)P, PtdIns(4,5)P_2 and PtdIns(3,4)P_2, which do not bind to SWAP-70 as seen in dot-blot analysis, also did not enhance the GEF activity (Supplementary Information Fig. S5b). Comparing the GEF activities of SWAP-70 and Sos revealed very similar levels of activity (Supplementary Information Fig. S5c). The GEF activity of an N-terminal deletion mutant that had retained only the DH domain was even higher than that of wild-type SWAP-70 (data not shown). This indicates that the DH domain alone is sufficient for GEF activity and that it might be regulated by interaction of the DH domain with other domains. A deletion mutant that lacks the C-terminal region inhibited membrane ruffling, indicating that it acted dominant-negatively (Fig. 2a). These results indicate that SWAP-70 is a PtdIns(3,4,5)P_3-dependent GEF for Rac and that this activity is correlated with the formation of membrane ruffles. Overexpression of SWAP-70 in COS7 cells resulted in an increase in activated Rac1 concentration, suggesting that SWAP-70 does indeed function as Rac-GEF *in vivo* (data not shown). Direct evidence for the activation of Rac1 *in vivo* was obtained by a pull-down assay specific for activated Rac (Fig. 3e). Only the wild type, but not any of the three SWAP-70 mutants, activated Rac1. Moreover, the dominant-negative C-terminal deletion mutant inhibited Rac1 activation. In contrast, no effect of SWAP-70 on Cdc42 activation was observed (data not shown). Because many of the conserved residues typical of known GEFs are substituted in SWAP-70, and the position of the PH domain is

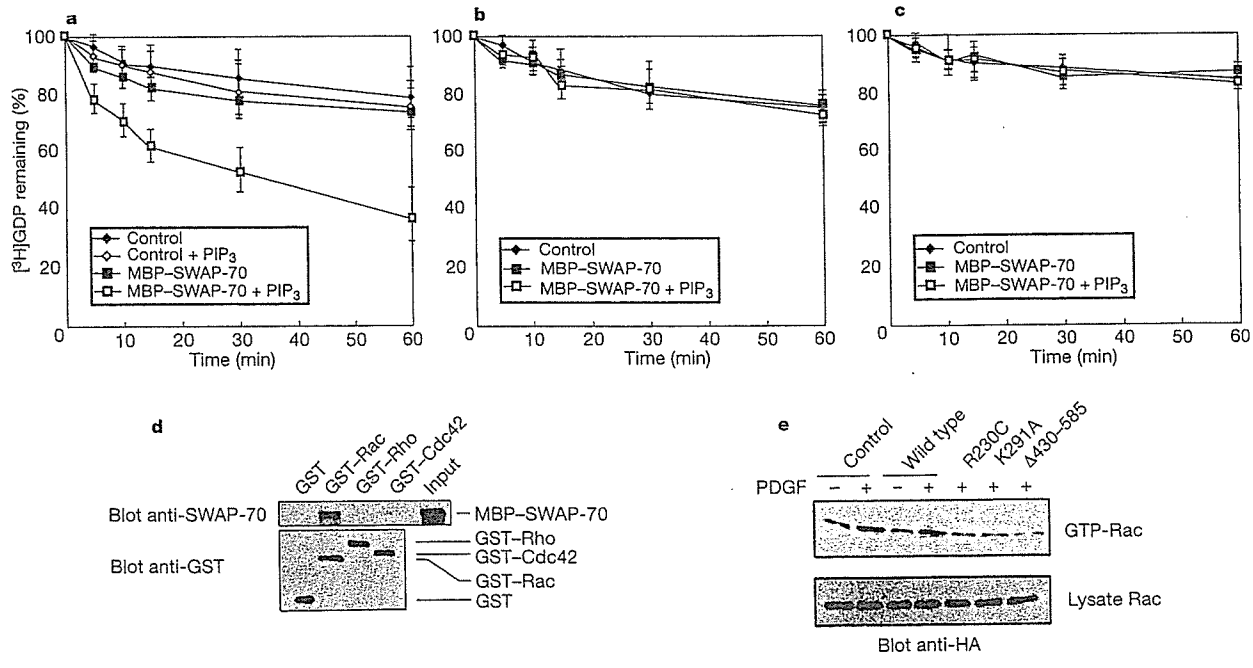

Figure 3 SWAP-70 is a PtdIns(3,4,5)P_3-dependent Rac specific GEF. **a–c**, GDP-release assays. [^{3}H]GDP-loaded Rac1 (**a**), RhoA (**b**) or Cdc42 (**c**) was incubated with MBP or MBP–SWAP-70 with or without PtdIns(3,4,5)P_3 (PIP$_3$) (1 μM). **d**, Binding of SWAP-70 to Rac1. Bead-bound GST–Rho GTPases were incubated with MBP–SWAP-70 (no Mg^{2+}). Complexes were analysed by immunoblotting with anti-SWAP-70 (top) or anti-GST-antibody (bottom). **e**, Inhibition of Rac1 by SWAP-70 mutants. NIH 3T3 cells expressing HA–Rac1 and a wild-type or a mutant GFP–SWAP-70, as indicated, were treated with (+) or without (–) PDGF. Lysates were incubated with GST–CRIB and detected with anti-HA antibody (top); bottom, cell lysates used.

different in other Rac-GEFs, we suggest that SWAP-70 is a new type of Rac-GEF.

To determine further the role of SWAP-70 *in vivo* in membrane ruffling induced by growth factors, kidney fibroblasts (or embryonic fibroblasts that yielded similar results) were cultured from wild-type or SWAP-70-deficient mice[11]. For ease of direct comparison with the earlier experiments (Figs 2 and 3), we chose fibroblasts although they express only low levels of cytoplasmic SWAP-70. SWAP-70 was detectable in wild-type cells but was absent from SWAP-70-deficient cells (data not shown). SWAP-70-deficient fibroblasts tended to show more stress fibres, and typical lamellipodia were rarely seen. The cells were less motile, forming tighter colonies than wild-type cells (data not shown). Wild-type cells responded to stimulation by EGF with membrane ruffling in more than 50% of the cells after 5–10 min (Fig. 4a, b). Wortmannin blocked this reaction. In contrast, membrane ruffling was significantly impaired in SWAP-70-deficient cells, as only up to 20% showed membrane ruffling (Fig. 4a, b). In these cells, stimulation with EGF was comparable to that in wild-type cells as judged by tyrosine phosphorylation of the EGF receptor and of other signalling molecules such as MAP kinase or Shc (Supplementary Information Fig. S6). Microinjection of an expression vector for SWAP-70 restored the ruffling deficiency to nearly the wild-type level (Fig. 4c; Supplementary Information Fig. S7). We also noted that high expression levels of SWAP-70 seem to inhibit ruffling in primary wild-type fibroblasts and (mildly) in NIH 3T3 cells. Taken together, these results confirm that SWAP-70 is important in the efficient induction of membrane ruffling in primary fibroblasts. As seen after the expression of mutant SWAP-70 (Fig. 3e), numbers of EGF-stimulated SWAP-70-deficient fibroblasts were significantly lower in Rac1 activation (Fig. 4d). SWAP-70 deficiency had no effect if ruffling was induced through PI(3)K-independent signals such as thrombin (Supplementary Information Fig. S8). Similarly, expression of the dominant-negative mutant R230C in NIH 3T3 cells did not block PI(3)K-independent ruffling induced by 12-O-tetradecanoylphorbol-13-acetate (data not shown). Taken together, these results indicate that SWAP-70 is a PI(3)K-dependent Rac-GEF, which receives signals from growth-factor receptors independently of Ras.

SWAP-70-deficient mice are vital and fertile, and no obvious phenotype other than deficient B-cell activation and dysfunctional mast cell biology have been reported[11,31]. Indeed, SWAP-70-deficient kidney cells still underwent membrane ruffling to some extent. These observations suggest that there might be alternative, SWAP-70-independent, pathways to activate Rac, perhaps through EGF- or PDGF-triggered activation of Ras. This is reminiscent of mice deficient in the Eps8 activator component of the Rac-GEF complex Eps8/E3b1/Sos-1 (ref. 25). PI(3)K- and Ras-dependent ruffling is impaired in the mutant, yet the mice are phenotypically healthy. Thus, indications exist *in vivo* for redundancies in Rac-dependent signalling of cytoskeletal rearrangements. □

Methods

Plasmids

KIAA0640 complementary DNA was provided by T. Nagase (Kazusa DNA Research Institute). For GFP–SWAP-70 expression in mammalian cells, cDNA of SWAP-70 was subcloned into pEGFP C1 (Clontech). Point mutations were induced by the QuickChange site-directed mutagenesis method (Stratagene). For the SWAP-70 (R230C and K291A) mutants, 5′-AAAACTGGACTGAATGTTGGTTTGTTTTAAAACCCAA-3′ and 5′-GATAAGACTTTTGAAATCAGTGCTAGCGATGCGAAGAAGAAACAGGAGTGGATT CAA-3′ were used as sense primers, respectively. For deletion mutants, cDNAs coding for different segments were inserted into pEGFP C1. pEFBOS HA–RasN17, pEFBOS HA–RasV12 and pEFBOS HA–Rac were gifts from K. Kaibuchi. pCMV HA–MAPK was

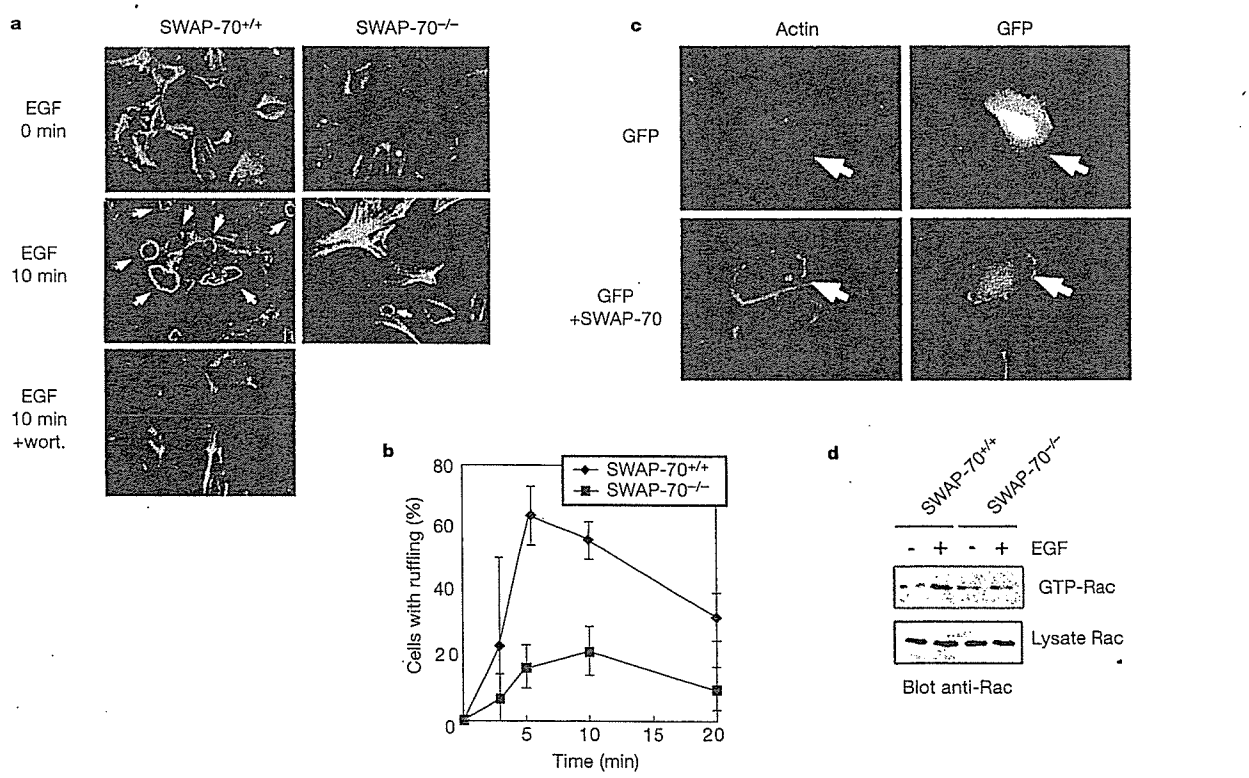

Figure 4 Impaired membrane ruffling in SWAP-70-deficient primary fibroblasts. **a**, Membrane ruffling induced by EGF (50 ng ml^{-1}). Cells were stained for F-actin. Arrows indicate cells with membrane ruffling. Wort., wortmannin. **b**, Scores of cells with membrane ruffling. **c**, Microinjection of an expression vector for SWAP-70 restores membrane ruffling. Scores of membrane ruffles in microinjected cells are shown. **d**, SWAP-70 regulates Rac activation *in vivo*. SWAP-70 wild-type (SWAP-70$^{+/+}$) or SWAP-70-deficient (SWAP-70$^{-/-}$) cells were treated with (+) or without (−) EGF. GTP-Rac1, precipitated from lysates with bead-bound GST–CRIB (top), or Rac1 in the lysate (bottom), was detected by immunoblotting with anti-Rac1 antibody.

provided by Y. Gotoh. cDNA of the GEF domain of human Sos1 was cloned by reverse-transcriptase-mediated polymerase chain reaction.

Protein purification and peptide sequence analysis

SWAP-70 purification from bovine brain with the use of PtdIns(3,4,5)P_3-APB beads and amino-acid sequencing were done as described[12,26].

Transfection

Transfection of COS7 cells was performed by electroporation. Cells were suspended in 500 µl of K-PBS (30.8 mM NaCl, 120.7 mM KCl, 8.1 mM Na_2HPO_4, 1.46 mM KCl, 5 mM $MgCl_2$) containing 20 µg DNA and were pulsed with a Cell-porator (Gibco BRL) at 800 µF capacitance and 240 V. Transfection of NIH 3T3 cells was done by electroporation as described above or by lipofection with LipofectAMINE (Gibco-BRL). Transfection of 293T cells was done as described previously[27]. Introduction of the DNA to cultivated kidney cells was done by microinjection as described previously[28] or by lipofection.

Fluorescence microscopy

Cells were stained for F-actin with tetramethylrhodamine-isothiocyanate-conjugated phalloidin as described previously[28]. Cells were examined by confocal fluorescence microscopy (Olympus IX-70).

GDP release assay for Rac, binding of SWAP-70 to Rac, and Rac activation assay

The GDP release assay was performed as described[29]. Binding of SWAP-70 to Rho GTPases was performed as described previously[30]. For the Rac1 (or Cdc42) activation assay, Rac1 (or Cdc42) was expressed in NIH 3T3, COS7 or primary kidney cells together with wild-type or mutant SWAP-70. Cells were treated for 5 min with or without PDGF or EGF, washed with ice-cold PBS containing 5 mM $MgCl_2$, lysed in lysis buffer (50 mM Tris-HCl pH 7.5, 1% (v/v) Triton X-100, 150 mM NaCl, 10% (v/v) glycerol, 2 mM dithiothreitol, 10 mM $MgCl_2$) and centrifuged for 10 min at 15,000*g* at 4 °C. Supernatants were incubated for 30 min at 4 °C with GST–Cdc42/Rac interactive binding (CRIB) (from PAK1), prebound to glutathione–Sepharose beads. Beads were washed, and bound material was analysed by SDS–polyacrylamide gel electrophoresis and immunoblotting.

Received 9 October 2001; accepted 11 February 2002.

1. Toker, A. & Cantley, L. C. Signalling through the lipid products of phosphoinositide-3-OH kinase. *Nature* 387, 673–676 (1997).
2. Downward, J. Role of phosphoinositide-3-OH kinase in Ras signaling. *Adv. Second Mess. Phosphoprot. Res.* 31, 1–10 (1997).
3. Martin, T. F. Phosphoinositide lipids as signaling molecules: Common themes for signal transduction, cytoskeletal regulation, and membrane trafficking. *Annu. Rev. Cell. Dev. Biol.* 14, 231–264 (1998).
4. Rameh, L. E. & Cantley, L. C. The role of phosphoinositide 3-kinase lipid products in cell function. *J. Biol. Chem.* 274, 8347–8350 (1999).
5. Fruman, D. A., Meyers, R. E. & Cantley, L. C. Phosphoinositide kinases. *Annu. Rev. Biochem.* 67, 481–507 (1998).
6. Fukui, Y., Ihara, S. & Nagata, S. Downstream of phosphatidylinositol-3 kinase, a multifunctional signaling molecule, and its regulation in cell responses. *J. Biochem. (Tokyo)* 124, 1–7 (1998).
7. Vanhaesebroeck, B. *et al.* Synthesis and function of 3-phosphorylated inositol lipids. *Annu. Rev. Biochem.* 70, 535–602 (2001).
8. Borggrefe, T., Wabl, M., Akhmedov, A. T. & Jessberger, R. A B-cell-specific DNA recombination complex. *J. Biol. Chem.* 273, 17025–17035 (1998).
9. Borggrefe, T. *et al.* Cellular, intracellular, and developmental expression patterns of murine SWAP-70. *Eur. J. Immunol.* 29, 1812–1822 (1999).
10. Masat, L. *et al.* Association of SWAP-70 with the B cell antigen receptor complex. *Proc. Natl Acad. Sci. USA* 97, 2180–2184 (2000).
11. Borggrefe, T., Keshavarzi, S., Gross, B., Wabl, M. & Jessberger, R. Impaired IgE response in SWAP-70-deficient mice. *Eur. J. Immunol.* 8, 2467–2475 (2001).
12. Shirai, R. *et al.* Synthesis of diacylglycerol analogs of phosphatidylinositol 3,4,5-trisphosphate. *Tetrahedron Lett.* 39, 9485–9488 (1998).
13. Staal, S. Molecular cloning of the *akt* oncogene and its human homologues AKT1 and AKT2: amplification of AKT1 in a primary human gastric adenocarcinoma. *Proc. Natl Acad. Sci. USA* 84, 5034–5037 (1987).
14. Tanaka, K. *et al.* A target of phosphatidylinositol 3,4,5-trisphosphate with a zinc finger motif similar to that of the ADP-ribosylation-factor GTPase-activating protein and two pleckstrin homology domains. *Eur. J. Biochem.* 245, 512–519 (1997).
15. Maekawa, M. *et al.* A novel mammalian Ras GTPase-activating protein which has phospholipid-binding and Btk homology regions. *Mol. Cell. Biol.* 14, 6879–6885 (1994).
16. Campbell, D. & Kernan, J. Mast cells in the central nervous system. *Nature* 210, 756–757 (1966).
17. Thomas, J. *et al.* Colocalization of X-linked agammaglobulinemia and X-linked immunodeficiency genes. *Science* 261, 355–358 (1993).
18. Han, J. *et al.* Role of substrates and products of PI 3-kinase in regulating activation of Rac-related guanosine triphosphatases by Vav. *Science* 279, 558–560 (1998).
19. Fleming, I. N., Gray, A. & Downes, C. P. Regulation of the Rac1-specific exchange factor Tiam1 involves both phosphoinositide 3-kinase-dependent and -independent components. *Biochem. J.* 351, 173–182 (2000).
20. Das, B. *et al.* Control of intramolecular interactions between the pleckstrin homology and Dbl homology domains of Vav and Sos1 regulates Rac binding. *J. Biol. Chem.* 275, 15074–15081 (2000).
21. Joly, M., Kazlauskas, A., Fay, F. S. & Corvera, S. Disruption of PDGF receptor trafficking by mutation of its PI-3 kinase binding sites. *Science* 263, 684–687 (1994).
22. Martin, S. S. *et al.* Phosphatidylinositol 3-kinase is necessary and sufficient for insulin-stimulated stress fiber breakdown. *Endocrinology* 137, 5045–5054 (1996).
23. Wennstrom, S. & Downward, J. Role of phosphoinositide 3-kinase in activation of ras and mitogen-activated protein kinase by epidermal growth factor. *Mol. Cell. Biol.* 19, 4279–4288 (1999).
24. Missy, K. *et al.* Lipid products of phosphoinositide 3-kinase interact with Rac1 GTPase and stimulate GDP dissociation. *J. Biol. Chem.* 273, 30279–30286 (1998).
25. Scita, G. *et al.* EPS8 and E3B1 transduce signals from Ras to Rac. *Nature* 401, 290–293 (1999).
26. Iwamatsu, A. S-carboxymethylation of proteins transferred onto polyvinylidene difluoride membranes followed by *in situ* protease digestion and amino acid microsequencing. *Electrophoresis* 13, 142–147 (1992).
27. Tanaka, K. *et al.* Evidence that a phosphatidylinositol 3,4,5-trisphosphate-binding protein can function in nucleus. *J. Biol. Chem.* 274, 3919–3922 (1999).
28. Kita, Y. *et al.* Microinjection of activated phosphatidylinositol-3 kinase induces process outgrowth in rat PC12 cells through the Rac-JNK signal transduction pathway. *J. Cell Sci.* 111, 907–915 (1998).
29. Lenzen, C., Cool, R. & Wittinghofer, A. Analysis of intrinsic and CDC25-stimulated guanine nucleotide exchange of p21ras-nucleotide complexes by fluorescence measurements. *Methods Enzymol.* 255, 95–109 (1995).
30. Zheng, Y., Bagrodia, S. & Cerione, R. Activation of phosphoinositide 3-kinase activity by Cdc42Hs binding to p85. *J. Biol. Chem.* 269, 18727–18730 (1994).
31. Gross, B. *et al.* SWAP-70 deficient mast cells are impaired in development and IgE-mediated degranulation. *Eur. J. Immunol.* (in the press).

Supplementary Information accompanies the paper on *Nature's* website (http://www.nature.com).

Acknowledgements

We thank B. Mayer and M. Matsuda for useful suggestions and critical reading of the manuscript, and T. Nagase (Kazusa DNA Research Institute) for supplying the KIAA0640 clone. This work was supported by grants-in-aid for scientific research to Y.F. from the Ministry of Education, Science, Sports, and Culture of Japan, and by an NIH grant to R.J.

Competing interests statement

The authors declare that they have no competing financial interests.

Correspondence and requests for materials should be addressed to Y.F. (e-mail: ayfukui@mail.ecc.u-tokyo.ac.jp).